

The Onset of Nuclear Structure Effects in Near-Barrier Elastic Scattering of Weakly-Bound Nuclei: ${}^6\text{He}$ and ${}^6\text{Li}$ Compared.

Y. Kucuk, I. Boztosun,

Department of Physics, Erciyes University, Kayseri, Turkey

N. Keeley

The Andrzej Soltan Institute for Nuclear Studies,

Department of Nuclear Reactions, ul. Hoża 69, 00-681 Warsaw, Poland

Abstract

The elastic scattering of the halo nucleus ${}^6\text{He}$ from heavy targets at incident energies near the Coulomb barrier displays a marked deviation from the standard Fresnel-type diffraction behavior. This deviation is due to the strong Coulomb dipole breakup coupling produced by the Coulomb field of the heavy target, a specific feature of the nuclear structure of ${}^6\text{He}$. We have performed Continuum Discretized Coupled Channels calculations for the elastic scattering of ${}^6\text{He}$ and ${}^6\text{Li}$ from ${}^{58}\text{Ni}$, ${}^{120}\text{Sn}$, ${}^{144}\text{Sm}$, ${}^{181}\text{Ta}$ and ${}^{208}\text{Pb}$ targets in order to determine the range of Z_T where this nuclear-structure specific coupling effect becomes manifest. We find that the strong Coulomb dipole breakup coupling effect is only clearly experimentally distinguishable for targets of $Z_T \approx 80$.

PACS numbers: 25.70.Bc, 21.60.Gx, 24.10.Eq

The interaction of two composite nuclei may lead to strong absorption in which the effects of coupling to non-elastic channels are dominant [1]. When strong absorption occurs, the scattering is primarily diffractive in nature and the elastic scattering cross section angular distributions will be of one of two types, characteristic of Fresnel or Fraunhofer diffraction, depending on the incident energy. Fresnel-type diffraction is observed at energies close to the Coulomb barrier when the Coulomb field acts like a diverging lens. As the incident energy is increased, the behavior of the angular distribution transforms from Fresnel- to Fraunhofer-type scattering where the Coulomb field is no longer effective as a diverging lens and interference between waves diffracted around opposite edges of the targets occurs, leading to the characteristic oscillatory behavior.

While stable nuclei usually exhibit one or other of these classical diffraction patterns in their elastic scattering angular distributions, the elastic scattering of the ${}^6\text{He}$ halo nucleus from heavy targets at near-barrier energies shows a strong deviation from the standard diffraction behavior. At these energies we would expect the elastic scattering to display the characteristic Fresnel-type diffraction pattern. However, a different structure is observed, in that the usual Coulomb rainbow peak is completely absent [2, 3]. The ${}^6\text{Li}$ nucleus shows a similar anomalous scattering for heavy targets at near-barrier incident energies but it is much weaker and considerably more difficult to observe experimentally, being a reduction of the Coulomb rainbow peak rather than a complete absence as for ${}^6\text{He}$, requiring very precise measurement of the elastic scattering angular distributions [4].

A similar deviation from the classical Fresnel diffraction pattern was initially observed experimentally in the elastic scattering of ${}^{18}\text{O} + {}^{184}\text{W}$ [5], and was interpreted as arising from the effect of strong Coulomb excitation of the first 2^+ state in the ${}^{184}\text{W}$ target. Strong Coulomb coupling effects are also responsible for the effect seen in the near-barrier elastic scattering of ${}^6\text{He}$ from heavy targets. When the atomic number of the target nucleus (Z_T) is large, the breakup of the weakly bound projectile is dominated by the Coulomb field. It is the large Coulomb dipole ($E1$) breakup probability of ${}^6\text{He}$ and the strong coupling of this process to the elastic scattering that causes the deviation for a ${}^6\text{He}$ projectile from the classical diffraction pattern. The elastic scattering of ${}^6\text{He}$ from the medium-mass ${}^{64}\text{Zn}$ target does not show this effect [3, 6], and appears similar to that for ${}^6\text{Li}$ from similar mass targets, presumably due to the reduced importance of the Coulomb breakup. For ${}^6\text{Li}$, the similar effect on the elastic scattering is caused by the virtual *quadrupole* ($E2$) breakup

coupling ($E1$ breakup is not allowed for the ${}^6\text{Li} \rightarrow \alpha + d$ process) and is consequently much weaker than for ${}^6\text{He}$ (with both $E1$ and $E2$ breakup allowed) and only apparent in precise measurements for heavy targets like ${}^{208}\text{Pb}$ at near-barrier energies. The elastic scattering of ${}^6\text{Li}$ therefore provides a good benchmark for comparison with ${}^6\text{He}$ elastic scattering.

It is not possible at present to easily control the beam energy of radioactive nuclei and thus optimize the experimental visibility of any interesting features that may arise due to the particular internal structure properties of these nuclei. For example, one feature of halo nuclei is the possibility of low-lying dipole strength, and this characteristic has been demonstrated experimentally and theoretically in the scattering of ${}^6\text{He}$ from ${}^{208}\text{Pb}$. The change observed in the elastic scattering is an interference between nuclear and Coulomb contributions that is highly dependent on the charge of the target nucleus and the beam energy relative to the Coulomb barrier. While it is not possible yet to predict all of the other types of behavior that might occur in exotic nuclei, exploring the virtual dipole effect as a function of bombarding energy and nuclear target charge theoretically for ${}^6\text{He}$ scattering can show the regime where one should look generally for these new effects and where the elastic scattering is sensitive to the details of the projectile nuclear structure.

In this note, we investigate over what range of Z_T the Coulomb dipole breakup virtual coupling effect is sufficiently important that the ${}^6\text{He}$ elastic scattering shows a measurable difference from the analogous ${}^6\text{Li}$ scattering and is therefore sensitive to its specific nuclear structure properties. For this purpose, we have calculated the elastic scattering of ${}^6\text{He}$ and ${}^6\text{Li}$ by different nuclei from ${}^{58}\text{Ni}$ to ${}^{208}\text{Pb}$ at energies near the Coulomb barrier using the Continuum Discretized Coupled Channels (CDCC) method. As the strong coupling effect is linked to the specific nature of the ${}^6\text{He}$ structure it is hoped that this study will prove useful in planning future radioactive beam experiments by helping to pinpoint the target and incident energy ranges where such structure-dependent effects are most clearly manifest.

We performed CDCC calculations for ten different systems, ${}^6\text{He}$ and ${}^6\text{Li} + {}^{58}\text{Ni}$, ${}^{120}\text{Sn}$, ${}^{144}\text{Sm}$, ${}^{181}\text{Ta}$ and ${}^{208}\text{Pb}$ in order to find a critical Z_T value where the ${}^6\text{He}$ elastic scattering is measurably different from that for ${}^6\text{Li}$. In order to remove trivial effects due to the difference in charge between ${}^6\text{Li}$ and ${}^6\text{He}$, calculations were compared for the same centre of mass energy relative to the Coulomb barrier, $E_{\text{c.m.}} - V_B$, where the Coulomb barrier height

V_B was calculated according to the relation [7]:

$$V_B = \frac{Z_P Z_T e^2}{R_P + R_T} \quad (1)$$

where $R = 1.16 A^{1/3} + 1.2$. While this relation overestimates the Coulomb barrier due to its neglect of the nuclear potential it should be adequate for our purposes. For each target, calculations were performed at two energies, corresponding to values of $E_{\text{c.m.}} - V_B$ of 1.005 and 5.534 MeV, equating to incident laboratory frame energies of 11.0 and 16.0 MeV for the ${}^6\text{He} + {}^{58}\text{Ni}$ system.

Although ${}^6\text{He}$ has a three-body $\alpha + n + n$ structure, assuming an $\alpha + {}^2n$ cluster structure can give physically meaningful results as the three-body wave function of the ${}^6\text{He}$ ground state has a large di-neutron (2n) component, which dominates the tail of the wave function [2, 8]. Thus, while the breakup of ${}^6\text{He}$ is best described by four-body models [9, 10, 11, 12, 13], their numerically demanding nature, combined with the lack of a generally available code able to implement such calculations make the use of standard three-body CDCC calculations attractive in a study of this kind. Therefore, CDCC calculations were performed using the modified two-body di-neutron model of ${}^6\text{He}$ proposed by Moro *et al.* [3], where the binding energy of the di-neutron in the ground state is increased to 1.6 MeV to give a wave function that well matches that of more physically sophisticated three-body models. This model describes very well the elastic scattering of ${}^6\text{He}$ for several targets covering the mass range studied here and gives a coupling effect similar to that of four-body CDCC calculations [3]. It is therefore adequate for our purposes in providing a good description of the elastic scattering of ${}^6\text{He}$, although it is not claimed to provide an accurate picture of the breakup cross section itself, merely its coupling effect on the elastic scattering. To calculate the interaction potentials the single-folding technique [14] was used and the necessary $\alpha +$ target, ${}^2n +$ target optical potential parameters were taken from Refs. [15] and [16], respectively, the latter being a global deuteron potential as 2n scattering potentials are obviously not available. The $\alpha + {}^2n$ binding potential was of Woods-Saxon form with parameters $R = 1.9$ fm and $a = 0.25$ fm [17].

The ${}^6\text{He}$ $\alpha + {}^2n$ continuum was discretized into bins of widths $\Delta k = 0.1 \text{ fm}^{-1}$ and up to a maximum excitation energy of $\epsilon = 7.7$ MeV in $\alpha + {}^2n$ relative momentum (k) space. The maximum value of k was chosen in each case so as to ensure convergence of the results, i.e. it was checked that adding an additional bin did not affect the result of the calculation. All non-

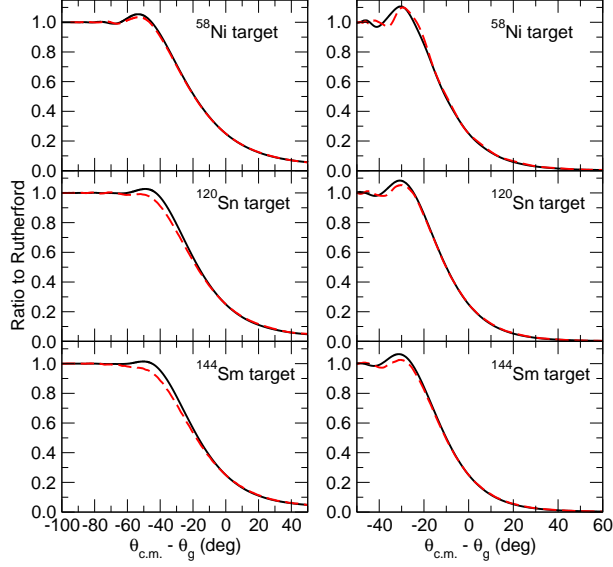


FIG. 1: (Color online) Angular distributions of differential cross section (ratio to Rutherford cross section) for ${}^6\text{He}$ (dashed curves) and ${}^6\text{Li}$ (solid curves) + ${}^{58}\text{Ni}$, ${}^{120}\text{Sn}$, and ${}^{144}\text{Sm}$ elastic scattering. The left-hand panels are for $E_{\text{c.m.}} - V_{\text{B}} = 1.005$ MeV and the right-hand panels for $E_{\text{c.m.}} - V_{\text{B}} = 5.534$ MeV.

resonant cluster states corresponding to $\alpha + {}^2n$ relative angular momenta $L = 0, 1, 2, 3$ were included as well as the 1.8 MeV 2^+ resonant state. The coupled equations were integrated up to $R = 80$ fm and used 200 partial waves for the projectile-target relative motion.

The ${}^6\text{Li}$ calculations were similar to those described in Ref. [18]. Again, the maximum value of k was chosen to ensure convergence. The $\alpha + \text{target}$ and $d + \text{target}$ potentials were also taken from Refs. [15] and [16], respectively. All calculations were performed using the code Fresco [19].

The results of the calculations are presented in Figs. 1 and 2, those for ${}^6\text{He}$ being denoted by the dashed curves and those for ${}^6\text{Li}$ by the solid curves. To emphasize the angular region around the Coulomb rainbow the cross section scales (expressed as a ratio to the Rutherford cross section) are linear. To remove any residual “geometric” differences the angular distributions are plotted as a function of $\theta_{\text{c.m.}} - \theta_{\text{g}}$, where θ_{g} is the grazing angle defined by the “quarter-point recipe”.

We immediately see that for a ${}^{58}\text{Ni}$ target ($Z_{\text{T}} = 28$) the calculated ${}^6\text{Li}$ and ${}^6\text{He}$ angular distributions are absolutely identical when plotted in this fashion; measurements of the elastic scattering from targets in this mass region are clearly not sensitive to the details

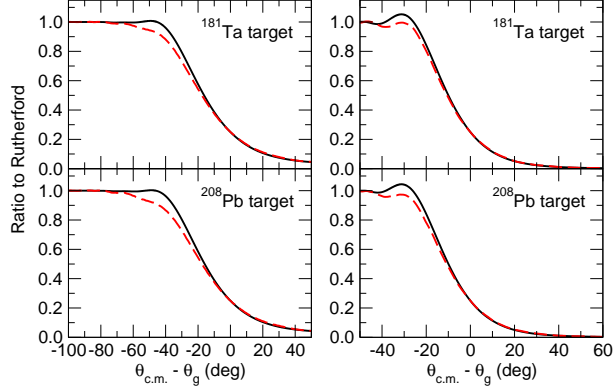


FIG. 2: (Color online) Angular distributions of differential cross section (ratio to Rutherford cross section) for ${}^6\text{He}$ (dashed curves) and ${}^6\text{Li}$ (solid curves) + ${}^{181}\text{Ta}$ and ${}^{208}\text{Pb}$ elastic scattering. The left-hand panels are for $E_{\text{c.m.}} - V_{\text{B}} = 1.005$ MeV and the right-hand panels for $E_{\text{c.m.}} - V_{\text{B}} = 5.534$ MeV.

of the nuclear structure of the projectile. For a ${}^{120}\text{Sn}$ target, while the calculated angular distributions are slightly different at $E_{\text{c.m.}} - V_{\text{B}} = 1.005$ MeV the difference is too small to be measurable; at $E_{\text{c.m.}} - V_{\text{B}} = 5.534$ MeV the ${}^6\text{He}$ and ${}^6\text{Li}$ angular distributions are again identical.

The magnitude of the structure-specific coupling effect for ${}^6\text{He}$ elastic scattering of course increases with increasing target charge, it being a consequence of strong Coulomb dipole coupling; thus for the ${}^{144}\text{Sm}$ target ($Z_{\text{T}} = 62$) a complete lack of a Coulomb rainbow is clearly observed for $E_{\text{c.m.}} - V_{\text{B}} = 1.005$ MeV, although any reasonable measurement would still be unable to detect any difference from the corresponding ${}^6\text{Li}$ angular distribution. The ${}^{144}\text{Sm}$ target also provides a good example of the dependence of the coupling effect on incident energy, as the calculated angular distribution for $E_{\text{c.m.}} - V_{\text{B}} = 5.534$ MeV is virtually identical to the ${}^6\text{Li}$ one. For a given target, as the incident energy is increased the coupling effect weakens and the Coulomb rainbow gradually manifests itself. This is a well-known general feature of Fresnel-type scattering for heavy ions; for ${}^6\text{He}$ scattering from a heavy target the effect is somewhat different as the Coulomb breakup coupling dominates at energies just above the Coulomb barrier to such an extent that the Coulomb rainbow is not merely absent but completely effaced.

In Fig. 2 the angular distributions for ${}^{181}\text{Ta}$ ($Z_{\text{T}} = 73$) and ${}^{208}\text{Pb}$ ($Z_{\text{T}} = 82$) targets show clear differences between ${}^6\text{He}$ and ${}^6\text{Li}$ at both values of $E_{\text{c.m.}} - V_{\text{B}}$. However, for the ${}^{181}\text{Ta}$

target the difference at $E_{\text{c.m.}} - V_{\text{B}} = 1.005$ MeV would be barely detectable in a measurement to a precision of ± 1 % for the the ${}^6\text{Li}$ elastic scattering and ± 2 % for the ${}^6\text{He}$ measurement (both achievable in a reasonable time scale with currently available beam intensities and detector arrays). The use of a Ta target is largely hypothetical in any case, as all the stable isotopes of this element have very low-lying excited states that make the measurement of pure elastic scattering impossible, even with stable beams. This problem also occurs for the other elements in the $Z = 70$ region, ruling out their practical use as targets in this type of study; we included a ${}^{181}\text{Ta}$ target in our study for the sake of completeness to check whether a (hypothetical) ideal target with a charge of around 70 would be sufficient to enable clear experimental separation of projectile structure-specific coupling effects in the elastic scattering.

With a ${}^{208}\text{Pb}$ target we finally see a clearly measurable difference between the ${}^6\text{He}$ and ${}^6\text{Li}$ elastic scattering angular distributions for $E_{\text{c.m.}} - V_{\text{B}} = 1.005$ MeV; at $E_{\text{c.m.}} - V_{\text{B}} = 5.534$ MeV the difference would just be detectable for measurements with a precision of ± 1 % and ± 2 % for ${}^6\text{Li}$ and ${}^6\text{He}$, respectively. Values of $E_{\text{c.m.}} - V_{\text{B}} = 1.005$ MeV correspond to incident ${}^6\text{Li}$ and ${}^6\text{He}$ energies of 33.06 MeV and 22.38 MeV, respectively for a ${}^{208}\text{Pb}$ target. Measured elastic scattering angular distributions for ${}^6\text{Li}$ and ${}^6\text{He} + {}^{208}\text{Pb}$ are available in the literature for incident energies of 33.0 MeV [4] and 22.0 MeV [20], enabling us to test the reliability of our calculations and the conclusions to be drawn therefrom. We plot them as a function of $\theta_{\text{c.m.}} - \theta_{\text{g}}$ in Fig. 3, together with the relevant CDCC calculations. Not only do they confirm the results of our calculations, but also the practicability of measuring the elastic scattering to sufficient precision to observe the predicted effect. The agreement between calculations and data is not perfect due to the use of global optical potentials as input in order to have a consistent set of results for several targets; slight adjustment of the potential well depths or the use of fitted potentials would enable perfect fits to be obtained. However, in the context of this work only qualitative agreement is required.

In summary, it has been shown by means of CDCC calculations that the large Coulomb dipole coupling effect observed in the elastic scattering of ${}^6\text{He}$ from ${}^{197}\text{Au}$ and ${}^{208}\text{Pb}$ targets at energies close to the Coulomb barrier [3] is only clearly evident, in the sense that the angular distribution is unambiguously experimentally distinguishable from that for ${}^6\text{Li}$, for targets with $Z_T \approx 80$. Furthermore, the incident energy must be close to the top of the nominal Coulomb barrier, that is to say a few MeV above the experimentally determined

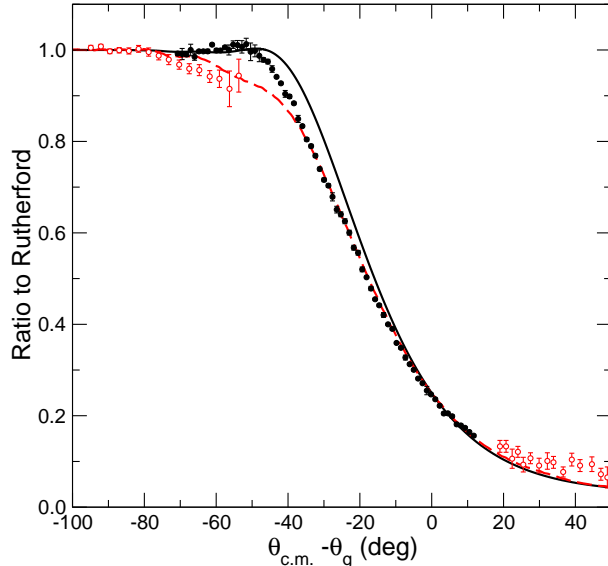


FIG. 3: (Color online) Experimental angular distributions of the differential cross section (ratio to Rutherford cross section) for ${}^6\text{He}$ (unfilled circles) and ${}^6\text{Li}$ (filled circles) elastic scattering from ${}^{208}\text{Pb}$ at incident energies of 22.0 MeV [20] and 33.0 MeV [4], respectively. Solid and dashed curves denote CDCC calculations for ${}^6\text{Li}$ and ${}^6\text{He}$ projectiles, respectively.

barrier (in the sense of the energy at which the measured elastic scattering cross section becomes equal to that for Rutherford scattering over the entire angular range).

The calculations presented here are specific to ${}^6\text{He}$ scattering. However, it is now well established that ${}^6\text{He}$ has a strong low-lying electric dipole strength in the $\alpha+n+n$ continuum, see e.g. [21], and that coupling to this strength is responsible for the characteristic appearance of the elastic scattering of ${}^6\text{He}$ from heavy targets [2, 3]. Low-lying continuum dipole strength is a property that is shared, or thought to be shared, with several other weakly-bound light radioactive nuclei, e.g. ${}^{11}\text{Li}$ and ${}^{11}\text{Be}$. While detailed comparison with models of the nuclei in question remains difficult due to the many-body nature of the problem (although progress is being made in this direction, see e.g. [9, 10, 11, 12, 13, 22, 23]) it should be possible to make qualitative conclusions concerning the relative strengths of these couplings by a comparison of the relevant near-barrier elastic scattering measurements. Extrapolation of the calculations presented here leads to the conclusion that future experiments to measure the elastic scattering of such nuclei should concentrate on heavy ($Z_T \approx 80$) targets — preferably ${}^{208}\text{Pb}$ or similar — at energies a few MeV above the Coulomb barrier for the systems concerned in order to maximize the structure dependence of the coupling effects.

Acknowledgments

This project is supported by the Turkish Science and Research Council (TÜBİTAK) with Grant No:107T824 and the Turkish Academy of Sciences (TÜBA-GEBİP). Y. Kucuk would also like to thank Prof. K. Rusek for the hospitality during her stay in Warsaw.

- [1] G. R. Satchler, *Direct Nuclear Reactions* (Oxford University Press, Oxford, 1983).
- [2] K. Rusek, N. Keeley, K.W. Kemper, and R. Raabe, *Phys. Rev. C* **67** (2003) 041604(R).
- [3] A.M. Moro, K. Rusek, J.M. Arias, J. Gómez-Camacho, and M. Rodríguez-Gallardo, *Phys. Rev. C* **75**, 064607 (2007).
- [4] N. Keeley, S.J. Bennett, N.M. Clarke, B.R. Fulton, G. Tungate, P.V. Drumm, J.S. Lilley, and M.A. Nagarajan, *Nucl. Phys.* **A571**, 326 (1994).
- [5] C.E. Thorn, M.J. LeVine, J.J. Kolata, C. Flaum, P.D. Bond, and J.-C. Sens, *Phys. Rev. Lett.* **38**, 384 (1977).
- [6] A. Di Pietro, P. Figuera, F. Amorini, C. Angulo, G. Cardella, S. Cherubini, T. Davinson, D. Leanza, J. Lu, H. Mahmud, M. Milin, A. Musumarra, A. Ninane, M. Papa, M.G. Pellegriti, R. Raabe, F. Rizzo, C. Ruiz, A.C. Shotter, N. Soic, S. Tudisco, and L. Weissman, *Phys. Rev. C* **69**, 044613 (2004).
- [7] P.E. Hodgson, *Nuclear Heavy-Ion Reactions* (Clarendon Press, Oxford, 1978), p. 2.
- [8] M.V. Zhukov, B.V. Danilin, D.V. Federov, J.M. Bang, I.J. Thompson, and J.S. Vaagen, *Phys. Rep.* **231** (1993) 151.
- [9] T. Matsumoto, E. Hiyama, K. Ogata, Y. Iseri, M. Kamimura, S. Chiba, and M. Yahiro, *Phys. Rev. C* **70**, 061601(R) (2004).
- [10] T. Matsumoto, E. Hiyama, M. Yahiro, K. Ogata, Y. Iseri, and M. Kamimura, *Nucl. Phys.* **A738**, 471 (2004).
- [11] T. Matsumoto, T. Egami, K. Ogata, Y. Iseri, M. Kamimura, and M. Yahiro, *Phys. Rev. C* **73**, 051602 (2006).
- [12] R. Chatterjee, P. Banerjee, and R. Shyam, *Nucl. Phys.* **A692** (2001) 476.
- [13] M. Rodríguez-Gallardo, J. M. Arias, J. Gómez-Camacho, R.C. Jhonson, A. M. Moro, I. J. Thompson, and J. A. Tostevin, *Phys. Rev. C* **77** (2008) 064609.

- [14] B. Buck and A.A. Pilt, Nucl. Phys. **A280** (1977) 133.
- [15] V. Avrigeanu, P.E. Hodgson, and M. Avrigeanu, Phys. Rev. **C49** (1994) 2136.
- [16] C.M. Perey and F.G. Perey, Phys. Rev. **132** (1963) 755.
- [17] K. Rusek, K.W. Kemper, and R. Wolski, Phys. Rev. **C64** (2001) 044602.
- [18] C. Beck, N. Keeley, and A. Diaz-Torres, Phys. Rev. C **75**, 054605 (2007).
- [19] I.J. Thompson, Comput. Phys. Rep. **7** (1988) 167.
- [20] A.M. Sánchez-Benítez, D. Escrig, M.A.G. Álvarez, M.V. Andrés, C. Angulo, M.J.G. Borge, J. Cabrera, S. Cherubini, P. Demaret, J.M. Espino, P. Figuera, M. Freer, J.E. García-Ramos, J. Gómez-Camacho, M. Gulino, O.R. Kakuee, I. Martel, C. Metelko, A.M. Moro, F. Pérez-Bernal, J. Rahighi, K. Rusek, D. Smirnov, O. Tengblad, P. Van Duppen, and V. Ziman, Nucl. Phys. **A803**, 30 (2008).
- [21] T. Aumann, D. Aleksandrov, L. Axelsson, T. Baumann, M.J.G. Borge, L.V. Chulkov, J. Cub, W. Dostal, B. Eberlein, Th. W. Elze, H. Emling, H. Geissel, V.Z. Goldberg, M. Golovkov, A. Grünschloß, M. Hellström, K. Hencken, J. Holeczek, R. Holzmann, B. Jonson, A.A. Korsheninikov, J.V. Kratz, G. Kraus, R. Kulesa, Y. Leifels, A. Leistenschneider, T. Leth, I. Mukha, G. Münzenberg, F. Nickel, T. Nilsson, G. Nyman, B. Petersen, M. Pfützner, A. Richter, K. Riisager, C. Scheidenberger, G. Schrieder, W. Schwab, H. Simon, M.H. Smedberg, M. Steiner, J. Stroth, A. Surowiec, T. Suzuki, O. Tengblad, and M.V. Zhukov, Phys. Rev. C **59**, 1252 (1999)
- [22] N.C. Summers, F.M. Nunes, and I.J. Thompson, Phys. Rev. C **73**, 031603 (2006).
- [23] N.C. Summers, F.M. Nunes, and I.J. Thompson, Phys. Rev. C **74**, 014606 (2006).